

Intrinsic Image Transfer for Illumination Manipulation

Junqing Huang, *Member, IEEE*, Michael Ruzhansky, *Member, IEEE*, Qianying Zhang, *Member, IEEE*,
Haihui Wang, *Member, IEEE*

Abstract—This paper presents a novel intrinsic image transfer (IIT) algorithm for illumination manipulation, which creates a local image translation between two illumination surfaces. This model is built on an optimization-based framework consisting of three photo-realistic losses defined on the sub-layers factorized by an intrinsic image decomposition. We illustrate that all losses can be reduced without the necessity of taking an intrinsic image decomposition under the well-known spatial-varying illumination illumination-invariant reflectance prior knowledge. Moreover, with a series of relaxations, all of them can be directly defined on images, giving a closed-form solution for image illumination manipulation. This new paradigm differs from the prevailing Retinex-based algorithms, as it provides an implicit way to deal with the per-pixel image illumination. We finally demonstrate its versatility and benefits to the illumination-related tasks such as illumination compensation, image enhancement, and high dynamic range (HDR) image compression, and show the high-quality results on natural image datasets.

Index Terms—Image illumination and reflectance, intrinsic image decomposition, intrinsic images transfer, illumination manipulation.

1 INTRODUCTION

IMAGE illumination is one of the basic and important cues for both human and computer vision. Shadows reveal black while highlights make white — visual objects look quite different under varying illumination conditions. The study of image illumination jointing with perception problems can be dated back to Helmholtz who had interpreted that human perception of the “intrinsic” property of scene is regardless of the light shed on it, which is also known as “lightness constancy” [35]. Although theories have been extensively studied over the past decades, as Gilchrist [19] pointed out, how human determines lightness, whiteness of a scene, like vision in general, remains a mystery. Recent analysis has also shown that human’s perception of lighting is deeply influenced by human vision system (HVS), which involves some, yet, not fully understood mechanisms, interactions, and a series of feedback [19].

The controlling of image illumination associated with intrinsic image decomposition has also received great attention because it helps to reduce the degradation of images in color, saturation, brightness, and contrast in many applications. It has been shown that a fine-balanced illumination condition is beneficial to a number of image processing and computer vision tasks, including illumination compensation, image enhancement and tone mapping, and high dynamic range (HDR) image compression, and so on. In the literature, tone mapping operators (TMO) [40], [42] and

Retinex-based image decomposition [5], [35] are two mainstream ways to these image illumination problems. TMO methods such as gamut mappings [40], [42] always treat image intensities as image illumination and adjust intensities (or hue, saturation) with specified tone-mapping curves. Most of them are simple and effective, but they may fail to produce high-quality details due to the limited ability in suppressing the potential noise and artifacts. The Retinex-based methods [15], [44], [46], in contrast, deal with image illumination under the Retinex theory [35]. They usually produce high-quality results with appropriate configurations but still have limitations in regularizing ill-posed intrinsic image decomposition, especially under the conditions of insufficient prior knowledge. In general, most of the existing methods can be interpreted under the famous Retinex theory [35], the core of which is how to make an intrinsic image decomposition, explicitly or implicitly, and then to manipulate or control the image illumination appropriately to achieve target purposes.

In this paper, we investigate a generalized intrinsic image model and its connection to image illumination manipulation. Specifically, we present an intrinsic image transfer (IIT) algorithm which implicitly creates a local image translation between two illumination surfaces. We illustrate that this IIT model can be beneficial for a wide range of illumination-related tasks in computer vision because they essentially share very similar illumination problems under an intrinsic image model. This model is built on an optimization framework consisting of three photorealistic losses derived from image illumination, reflectance and content, respectively. Initially, each loss is defined on the sub-layers factorized by an intrinsic image model. For simplification, all of them are reduced and directly defined on images instead of the sub-layers based on the spatial-varying illumination and illumination-invariant reflectance prior knowledge. As we demonstrate below, all losses can be reduced into quadratic forms with a series of relaxations, thereby giving a closed-form solution for illumination manipulation. This new paradigm significantly differs from many existing Retinex-based methods, because it provides a way to deal

- J. Huang and M. Ruzhansky are with the Department of Mathematics: Analysis, Logic and Discrete Mathematics, Faculty of Sciences, Ghent University, Ghent 9000, Belgium (e-mail: Junqing.Huang@UGent.be; Michael.Ruzhansky@UGent.be).
- Q. Zhang is with the Shenzhen Institute of Information Technology, Shenzhen 518172, China (e-mail: zhang_qy@sz.jnu.edu.cn).
- H. Wang is with the school of Mathematical Sciences, Beihang University, Beijing 100191, China (e-mail: whhmath@buaa.edu.cn).

Manuscript received XX, XXXX, 2021; revised XX, XXXX, 2021; accepted XX, XXXX, 2021. Date of publication XX, XXXX, 2021; date of current version XX, XXXX, 2021. (Corresponding author: Haihui Wang.)

Recommended for acceptance by XXXX.

Digital Object Identifier no. XX.XXXX/TPAMI.XXXX.XXXXXXX

with image illumination without the necessity of taking an ill-posed intrinsic image decomposition. Moreover, this method has an excellent ability in simultaneously preserving locally consistent structures and suppressing artifacts such as halos and textural distortions. The major contributions are summarized as follows:

- A generalized minimization framework is concisely designed for image illumination manipulation, where the photorealistic illumination, reflectance, and content losses are defined and reduced on the premise of spatial-varying illumination and illumination-invariant reflectance prior knowledge.
- A local translation-invariant encoding model based on the locally linear embedding (LLE) algorithm [47] is introduced to identify the illumination-invariant property of reflectance layer. This local model enables us to control the “intrinsic” reflectance layer directly without taking an ill-posed image decomposition.
- A series of applications are presented under our IIT model. All photorealistic losses are reduced into quadratic forms with the aid of an extra “exemplar” image, thereby giving a closed-form solution to image illumination manipulation.

Furthermore, our IIT algorithm takes a small step toward clarifying the relationship of different “intrinsic” layers under the Retinex-like models. As interpreted in Sec. 3 and 4, we present a new paradigm to regularize the “intrinsic” layers based on the photorealistic losses defined on images, which avoids the intrinsic image decomposition and simplifies the controlness of image illumination. To validate its versatility, we show experimental results on several illumination-related tasks: illumination compensation, image enhancement, and HDR image compression.

The paper is organized as follows. In Section 2, we discuss the related work. Our IIT algorithm is presented in Section 3. A generalized intrinsic image model and its connections to image illumination manipulation are discussed in Section 3.1 and 3.2, respectively. The methodology, together with three photorealistic losses, is systemically explored in Section 3.3. In Section 4, a series of experimental results are presented with the quantitative evaluation on different datasets. In Section 5, we draw our concluding remarks and future directions.

2 RELATED WORK

In the literature, many computational models have been proposed to explore the gap between the recorded color images and human visual perception of a natural scene. Previous work in image illumination manipulation covers a wide range of techniques. Despite the different generalization and forms, they commonly share a similar illumination problem that tone an ill-lighted image into a balanced one and bring out more visual information. We here mainly review some “intrinsic” image decomposition models and also investigate the connections and potential benefits to image illumination manipulation.

Retinex theory [35] is an early computational model proposed by Land and McCann to interpret the well-known “lightness constancy” phenomenon. In Retinex theory, it is usually assumed a Mondrian-like image that can be formulated by the point-wise multiplication of two components (illumination and reflection layers). The illumination layer measures the amount of incident light illuminated on an object; while the reflectance layer depicts the reliable visual information despite the varying illumination. Retinex theory shows how human visual mechanism performs the comparison of scenes to create the sensation of lightness. Based

on Retinex theory, Land [33] also derived a simple algorithm that classifies the strong gradients of an image into reflectance layer and all the other variations into illumination layer. Horn [23] interpreted that a complete image decomposition of them can be achieved by solving a Poisson equation mathematically. Due to its simplicity and effectiveness, it has been used as a bias for many illumination-related tasks such as illumination compensation, image enhancement, and high dynamic range (HDR) image compression. For example, Jobson [34] explored the properties of the center/surround function and proposed a so-called center/surround Retinex for dynamic range compression. The work was then extended to the classic multiscale Retinex [29] for color, contrast and brightness correction. Fattal [15] also proposed a high dynamic range compression method based on Retinex theory in the gradient domain of images. It has also stimulated many computational models, including the variational-based image decomposition [16], [30], [39], PDE-based image smoothing [23], to clarify the relationship of two components, as well as the benefits to the above illumination-related tasks. More recently, Elad [13] justified the relationship between a regularized Retinex and the bilateral filter [53] theoretically by characterizing the spatial-varying illumination, which also stimulates the use of edge-aware image filters [7], [14], [53] for image enhancement, HDR image compression, and so on.

Simultaneously, these methods that strive to decompose an image into different “intrinsic” components have drawn great attention with the terminology “intrinsic images” introduced by Barrow and Tenenbaum [5]. This type of technique is always known as intrinsic image decomposition, which, in nature, share similar Retinex-based assumptions. In general, it is a highly under-constrained problem to recover the multiple intrinsic layers from single or multiple images. In order to solve it, different assumptions, including sparse prior knowledge [21], [51], low-rank [24], [58] and non-local cues [57], [60] have been proposed to give guidance for image decomposition. Rother, et al. [46], for example, gave an image decomposition method by encoding the sparsity of the reflectance with a Gaussian mixture model. Bell, et al. [6] presented a dense conditional random field algorithm for intrinsic image decomposition on a large-scale indoor dataset. Recently, more complex computational models were proposed for real-world image decomposition. In [38], depth cues with RGB-D cameras were used to infer the intrinsic images. Jeon, et al. [27] introduced an image decomposition model based on locally linear embedding algorithm [47], which is related to our model but mainly strives to explicitly decompose an image into shading, reflectance and texture layers. Barron and Mailik [4] also formulated a similar one called “shape, albedo, and illumination from shading (SAIFS)” to recover each intrinsic layer from an image. Instead, Guo, et al. [21] proposed a model for low-light image enhancement that takes only illumination layer into account under dark channel prior. Notice that these decomposition-based methods always use a layer-remapping operator as an indispensable post-processing step to manipulate the image illumination; however, it is easy to introduce artifacts because the layer-remapping is out of the constraints of the intrinsic image decomposition.

Besides, recent advances in learning-based methods achieve a milestone for the overwhelming results in many challenging benchmarks [6], [12], [18], [26], [32]. Strongly benefiting from the deep convolutional neural networks (CNN) [20], [32], more and more delicate network architectures are springing out. It has also witnessed the use of deep learning approaches [11], [17],

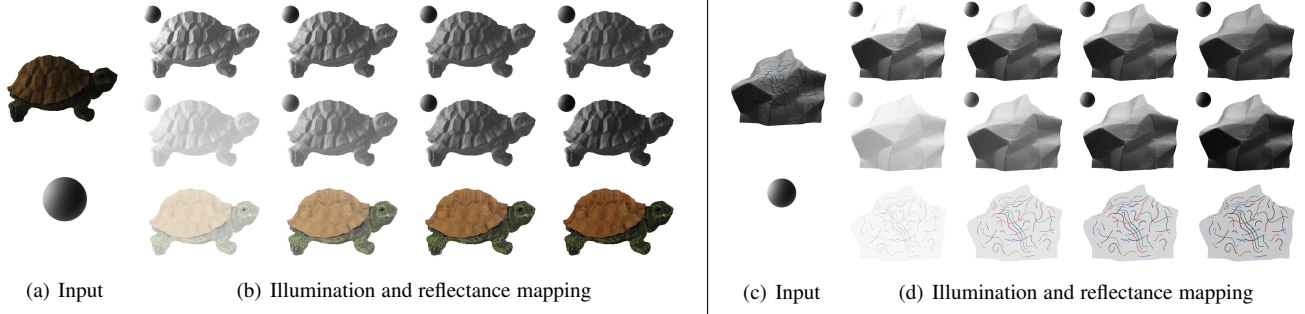


Fig. 1. Illumination and reflectance mapping in the logarithm domain. Top: global illumination mapping ($a = [0.3, 0.1, -0.1, -0.3]$), middle: local illumination mapping ($b = [0.6, 0.9, 1.1, 1.4]$), bottom: local reflectance mapping ($c = [0.5, 0.8, 1.2, 1.5]$).

[22], [36], [41] to explore and infer the intrinsic layers from single or multiple images or directly recover image illumination for better visual perception or interpretation. For example, Narihira et al. [43] firstly introduced deep learning to learn albedo from MPI Sintel dataset [8]. Chen et al. [9] recently released a new end-to-end training model with a fully convolutional network for the low-light images by using raw images for training. Andrey, et al. [25] presented an end-to-end weakly supervised photo enhancer (WESPE) to enhance an image automatically. Yet, one of the bottlenecks of these deep learning-based methods is the necessity of a large scale of high-quality matched training pairs for supervision. More recently, deep learning methods on unpaired datasets for image enhancement and tone mapping [10], [28], inspired by unsupervised image-to-image translation [59], bring new hope for easy and flexible image enhancement on real-world low-light images. The reader is referred to a systematic review and evaluation of existing deep learning-based low-light enhancement algorithms [37].

3 METHODOLOGY

In this section, we formulate our IIT algorithm under a well-known intrinsic image model and show how to derive and reduce the three photorealistic losses under this new model mathematically.

3.1 Intrinsic Images Model

Considering the Retinex model [5], we also assume that an image \mathcal{I} can be factorized into illumination \mathcal{L} and reflectance \mathcal{R} ,

$$\mathcal{I} = \mathcal{L} \odot \mathcal{R}, \quad (1)$$

where \odot is a point-wise multiplication operator, \mathcal{L} represents the light-dependent properties such as shading, shadows or specular highlights and \mathcal{R} represents material-dependent properties, known as the reflectance of a scene. In Eq. (1), \mathcal{L} and \mathcal{R} take rather different roles in controlling the image color, contrast, brightness and so on. In general, illumination \mathcal{L} is assumed to have a spatial-smoothing property and determines the visibility of a scene, while reflectance \mathcal{R} possesses illumination-invariant property and is expected to be piece-wise constant under varying lighting conditions. We here take the same terminologies: illumination and reflectance as interpreted [33] but each of them can be slightly different based on the concrete assumptions. It worthy to note that such assumptions have formed a basis for many existing intrinsic image decomposition algorithms [6], [23], [33], [46].

3.2 Multiple Observations

Considering an imaging system under varying lighting conditions, the captured images or videos could be severely degraded for the imbalance of illumination. As aforementioned, the solution to this illumination problem may arise from tonal adjustments [40], [42] to Retinex-based image decomposition [5], [35]. Despite the different forms, the main idea can be understood under Eq. (1) similarly. For tonal adjustments, image intensities are simply used as image illumination, and tone mapping methods are then employed to adjust the image illumination, which is simple and efficient for the no need of decoupling an image into layers. While these Retinex-based methods may take more complex steps: intrinsic image decomposition, layer-remapping, and image reconstruction for image illumination manipulation. Before going further, we show how each layer determines the change of an image under the assumption of Eq. (1).

For simplification, we consider Eq. (1) with the additive form in the logarithmic domain [46]. We denote \mathcal{I} , \mathcal{L} and \mathcal{R} as the logarithm of \mathcal{I} , \mathcal{L} and \mathcal{R} , respectively. The target image $\hat{\mathcal{I}}$ is represented as $\hat{\mathcal{I}} = a + b\mathcal{L} + c\mathcal{R}$. Obviously, the color, brightness, and contrast of the image $\hat{\mathcal{I}}$ are greatly affected by the parameters a , b , and c . As shown in Fig. 1, the brightness of illumination increases globally when adding a constant a to \mathcal{L} , but varies locally when multiplying it by a constant b ; while the contrast of an image significantly varies by multiplying \mathcal{R} with a constant c . We here attribute that the additive constant a has only impact on image illumination instead of reflectance, because \mathcal{R} is always assumed to be illumination-invariant under an intrinsic image model. In other words, it holds $c = 1$ unless in some cases the image contrast needs to be changed by adjusting the reflectance layer.

The above procedure, in nature, is widely adopted by many illumination-related methods such as illumination compensation, image enhancement and tone mapping, HDR image compression, and so on. However, such a diagram may lead to drawbacks due to the facts: (a) Intrinsic image decomposition is a highly ill-posed problem, and the results of which may highly dependent on prior knowledge. (b) It is not easy to determine an appropriate layer-remapped operator for both illumination and reflectance layers even providing high-quality decomposition results. (c) The artifacts introduced by the layer-remapping operator and image construction not easy to control, as they are out of the procedure of intrinsic image decomposition. In contrast, we illustrate that all the above steps can be integrated into a generalized optimization framework without the necessity of taking an ill-posed intrinsic

image decomposition. The idea is mainly derived from the famous spatial-varying illumination and illumination-invariant reflectance [46] with the following assumptions:

- Spatial-smoothing illumination, that is, illumination L is smoothing and dramatic variations in image, for example, strong or salient edges, textures and structures are mainly attributed to the reflectance R . Human vision system is not so sensitive to the absolute variations of illumination as that of reflectance for the “color-consistency” phenomenon.
- Illumination-invariant reflectance — that is to say, image reflectance R tends to be invariant under varying illumination conditions. It is also straightforward to claim that these local geometric structures formed by these dramatic variations in R have the same illumination-invariant property.
- The visibility of an image is primarily determined by image illumination L , whose intensities may need to be, locally or globally, compensated or adjusted for its discrepancy to the target, especially under varying illumination conditions.

The three terms enable us to handle image illumination in a rather flexible way. The first term suggests that image illumination L has a spatial-smoothing property and can be approximated with smoothing filtering methods; while image reflectance R contains abundant features and thus it can be constrained by regularizing these features equivalently. The second term implies that image reflectance R should be invariant when image illumination is compensated or adjusted, for example, taking a layer-remapping operator for image enhancement. In other words, the reflectance layer just shifts from one illumination surface to another one and has a spatial translation-invariant property. The last term indicates that image illumination L should approximate to a balanced one rather than the source for some image illumination applications, which also motivates us to introduce a new image, exemplar, to provide an illumination prior in these applications.

3.3 Illumination Manipulation Model

We now elaborate a generalized illumination manipulation model under the model of intrinsic images in Eq. (1), and investigate the potential benefits to a class of illumination-related tasks in computer vision. Let $\mathbf{s} = \{s_i\}_{i=1, \dots, N}$ be an input image, we illustrate the target output image $\mathbf{o} = \{o_i\}_{i=1, \dots, N}$, can be expressed as an optimal solution of the minimization problem,

$$\min_{\mathbf{o}} E(\mathbf{o}) = \alpha E^l(\mathbf{o}) + \beta E^r(\mathbf{o}) + \gamma E^c(\mathbf{o}), \quad (2)$$

where photorealistic loss E includes three terms E^l, E^r and E^c which are defined on illumination, reflectance and content respectively. The global parameters α, β, γ control the balance of three terms.

Illumination loss: In many illumination manipulation tasks, the degraded image is usually has a local or global illumination discrepancy to that of the target image. Considering this remarkable changeability of image illumination, it is generally unappropriated to fit the target output illumination \mathbf{o}^l to that of the source image. Instead, we impose \mathbf{o}^l to be close to a latent illumination surface \mathbf{c}^l . As a consequence, $E^l(\mathbf{o})$ can be defined as the distance between the two illumination layers,

$$E^l(\mathbf{o}) = \sum_i (o_i^l - c_i^l)^2, \quad (3)$$

where o_i^l and c_i^l are the i -th pixel illumination of output and exemplar, respectively; and the index l represents that Eq. (3) is done on the illumination layers.

Notice that Eq. (3) defines on the sub-layers \mathbf{o}^l and \mathbf{c}^l . We can now continue in two directions: we either aim at these latent illumination layers, which would returns to the problem of intrinsic image decomposition, or we reduce the loss to avoid the image decomposition. We here follow the second approach for simplification. Recalling the spatial-smoothing property of image illumination, we use filtering operators and treat the smoothing results as the illumination layers. Considering a Gaussian-like kernel \mathcal{K} , the illumination \mathbf{o}_i^l can be represented as a weighted sum of that of the neighbors $\{o_j\}_{j \in \mathcal{N}_i}$,

$$\begin{aligned} o_i^l &= \sum_{j \in \mathcal{N}_i} \mathcal{K}_{i,j} o_j, \quad \sum_{j \in \mathcal{N}_i} \mathcal{K}_{i,j} = 1, \\ \mathcal{K}_{i,j} &\propto \exp\left(-\frac{1}{\delta_{\mathbf{f}}^2} \|\mathbf{f}_i - \mathbf{f}_j\|_2^2\right), \end{aligned} \quad (4)$$

where \mathcal{N}_i denotes a neighbor set of pixel i , $\mathcal{K}_{i,j}$ is the Gaussian kernel weight between the pixel i and j ; and \mathbf{f} is a feature vector with standard deviation $\delta_{\mathbf{f}}$. \mathbf{f} can be the pixel’s position, intensity, chromaticity or abstract features. We now return to Eq. (3) and suggest that $E^l(\mathbf{o})$ can be represented by enforcing the smoothing outputs to be close to each other, that is,

$$E^l(\mathbf{o}) = \sum_i \sum_{j \in \mathcal{N}_i} (\mathcal{K}_{i,j}^o o_j - \mathcal{K}_{i,j}^c c_j), \quad (5)$$

where $\mathcal{K}_{i,j}^o$ and $\mathcal{K}_{i,j}^c$ are filter kernels. As we can see, Eq. (5) is identical to Eq. (3) in measuring the illumination loss under the spatial-smoothing illumination assumption. This relaxation thus avoids the tedious illumination separation and reduces the complexity of the algorithm significantly.

We call the image c in Eq. (5) as an “exemplar” image and show it is easy to generate a suitable exemplar for many illumination-related tasks. Notice that, on the one hand, the exemplar c is introduced to improve the degraded illuminations, therefore it should have consistent global illumination as that of the target image; on the other hand, the local details in c would be smoothed by kernel \mathcal{K} in Eq. (5), that is to say, the high-quality local details is not necessary for exemplar c . Considering the two points, we claim that it is commonly sufficient for image c to have a balanced global illumination, while the high-quality local details are not prerequisites for the image illumination loss. This conclusion will be also verified by a series of examples in the experiments.

Reflectance loss: Recall the illumination-invariant property of reflectance layers, the output reflectance \mathbf{o}^r is expected to be identical to, \mathbf{s}^r , that of the original image. We thus define $E^r(\mathbf{o})$ as the distance of them,

$$E^r(\mathbf{o}) = \sum_i (o_i^r - s_i^r)^2, \quad (6)$$

where s_i^r and o_i^r are the corresponding i -th pixels values of the reflectance layers. Clearly, Eq. (6) also requires an image decomposition as mentioned for Eq. (3).

Under the assumptions in Section 3.2, the reflectance layer of an image contains abundant features such as the salient edges, lines, and textures. These embedded features have the same illumination-invariant property, as they are only determined by the reflectance layers. This observation motivates us to regularize the reflectance by constraining these features. Mathematically, we first use a local linear model to encode these features, that is,

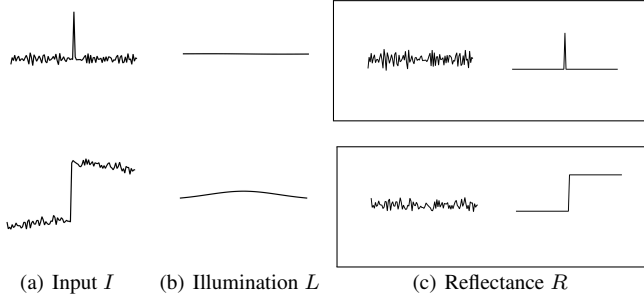


Fig. 2. The 1-D signal I is decomposed into three components: a spatial-varying L , a detail texture layer and a salient edge. We attribute the texture and edge to the reflectance R in our intrinsic image model.

$$s_i^r = \sum_{j \in \Omega_i} \omega_{i,j}^{s^r} s_j^r, \quad (7)$$

where Ω_i is a neighbor of pixel i and the weight satisfies $\sum_{j \in \Omega_i} \omega_{i,j}^{s^r} = 1$. The main idea of the Eq. (7) is to encode the pairwise relationship of the points s_i^r and its neighbors s_j^r into weights $\omega_{i,j}^{s^r}$. It is based on a plausible intuition that if the reflectance s^r keeps invariant, the weight $\omega_{i,j}^{s^r}$ is invariant as well. By analogy with the output \mathbf{o}^r , the photorealistic reflectance loss can be reformulated into the following constraints equivalently,

$$\begin{cases} \omega_{i,j}^{o^r} = \omega_{i,j}^{s^r}, \\ o_i^r = \sum_{j \in \Omega_i} \omega_{i,j}^{o^r} o_j^r, & \sum_{j \in \Omega_i} \omega_{i,j}^{o^r} = 1, \\ s_i^r = \sum_{j \in \Omega_i} \omega_{i,j}^{s^r} s_j^r, & \sum_{j \in \Omega_i} \omega_{i,j}^{s^r} = 1. \end{cases} \quad (8)$$

where $\omega_{i,j}^{o^r}$ and $\omega_{i,j}^{s^r}$ represent the weights, and the up-index s^r and o^r denote that the local linear “encoding” operators are acted on the reflectance layers. In the Eq. (8), we force $\omega_{i,j}^{o^r} = \omega_{i,j}^{s^r}$ to give a structural-consistency constraint for the reflectance layers. Although Eq. (6) and Eq. (8) have very different forms, they essentially play equivalent roles in constraining the reflectance layers.

Recall the spatial-varying illumination again, we have $s_k^l \approx \bar{s}_k^l$, where \bar{s}_k^l is mean illumination value in patch k . Besides, if two patches i and j are close to each other, we also have $\bar{s}_i^l \approx \bar{s}_j^l$. As shown in Fig. 2, they are clearly valid in the flat regions, and still hold true in the non-flat area, when salient variations (such as edges and textures) are attributed to the reflectance layers. Putting them into Eq. (7), we reduce the “encoding” model into

$$\begin{aligned} s_i &= (s_i^r + \bar{s}_i^l) \approx (s_i^r + \bar{s}_j^l) = \left(\sum_{j \in \Omega_i} \omega_{i,j}^{s^r} s_j^r + \bar{s}_j^l \right) \\ &= \sum_{j \in \Omega_i} \omega_{i,j}^{s^r} (s_j^r + \bar{s}_j^l) \approx \sum_{j \in \Omega_i} \omega_{i,j}^{s^r} (s_j^r + \bar{s}_j^l) \\ &\approx \sum_{j \in \Omega_i} \omega_{i,j}^{s^r} (s_j^r + \bar{s}_j^l) = \sum_{j \in \Omega_i} \omega_{i,j}^{s^r} s_j. \end{aligned} \quad (9)$$

The Eq. (9) illustrates that $\omega_{i,j}^{s^r}$ keeps invariant when adding a constant \bar{s}_i^l to the patch i , which makes sense for the translation-invariant property. In other words, the local linear model in Eq. (7) is also applicable to the image itself in views of the spatial-smoothing illumination, and we can regularize the reflectance directly without the necessity of decoupling the reflectance from

the image. Putting Eq. (7) and (9) into Eq. (8), $E^r(\mathbf{o})$ can be rewritten as,

$$\begin{aligned} E^r(\mathbf{o}) &= \sum_i (o_i - \sum_{j \in \Omega_i} \omega_{i,j}^o o_j)^2 \\ \text{s.t. } \omega_{i,j}^o &= \omega_{i,j}^s, \quad s_i = \sum_{j \in \Omega_i} \omega_{i,j}^s s_j, \end{aligned} \quad (10)$$

where $\omega_{i,j}^s = \omega_{i,j}^{s^r}$ and $\omega_{i,j}^o = \omega_{i,j}^{o^r}$ are the local “encoding” weights. The relationship between Eq. (8) and Eq. (10) is clear, as the second constraint in Eq. (8) is chosen as the objective function and the others act as constraints.

The models in Eq. (7) and Eq. (9) can be interpreted as locally linear embedding (LLE) [47] which was originally proposed for nonlinear dimensionality reduction. Due to its translation-invariant property, the LLE model enable us to translate the reflectance layer from source illumination surface to that of exemplar, while keeping the reflectance layer from changing. This property contributes the core of our whole illumination manipulation scheme.

Content loss: As aforementioned, the exemplar is used to provide global illumination prior. It maybe suffers from slight over-stretched illumination in the extreme cases, because it is usually provided by a very simple method, for example, CLAHE [61]. In order to avoid this illumination-overfitting, we additionally introduce a content loss $E^c(\mathbf{o})$ to regularize the global illumination. Here, we formulate $E^c(\mathbf{o})$ simply as the point-wise Euclidean distance between \mathbf{o} and \mathbf{s} ,

$$E^c(\mathbf{o}) = \sum_i (o_i - s_i)^2. \quad (11)$$

Recall the illumination-invariant reflectance prior, it is easy to see that Eq. (11) primarily acts on the illumination layers¹. In some situations, it is valuable for content loss to avoid potential illumination-overfitting. It is interesting to note that $E^c(\mathbf{o})$ plays an auxiliary role to prevent output illumination from being over-dependent on exemplars.

3.4 Optimization

Eventually, we combine three loss functions and rewrite Eq. (2) in a matrix form:

$$\begin{aligned} E(\mathbf{o}) &= \alpha \| \mathbf{K}^o \mathbf{o} - \mathbf{K}^c \mathbf{c} \|_2^2 + \beta \| \mathbf{M} \mathbf{o} \|_2^2 + \gamma \| \mathbf{o} - \mathbf{s} \|_2^2, \\ \text{s.t. } \omega_{i,j}^o &= \omega_{i,j}^s, \quad s_i = \sum_{j \in \Omega_i} \omega_{i,j}^s s_j, \end{aligned} \quad (12)$$

where $\mathbf{K}^o(\mathbf{K}^c)$ is an affinity matrix, whose (i, j) th entry is $\mathcal{K}_{i,j}^{o(c)}$; and $\mathbf{M} = [\mathbf{I} - \mathbf{W}]$ is a sparse coefficient matrix with identity \mathbf{I} and weight \mathbf{W} containing entries $\omega_{i,j}^o$. Once \mathbf{K}^o , \mathbf{K}^c and \mathbf{W} are pre-computed, the output image can be reconstructed by solving the Eq. (12) directly.

We first compute the filter kernel \mathcal{K} . In fact, different kernels can be configured in our framework. The simplest case can be the 2-D Gaussian filter (GF), where \mathbf{f} relies on pixel’s position: $\mathbf{p} = [p_x, p_y]$ with the x and y directional coordinates p_x and p_y respectively. One can use bilateral filter (BF) [53] for more robust results, which considers both the pixel’s position $\mathbf{p} = [p_x, p_y]$ and color intensities (R_i, G_i, B_i) . We set $\delta_{\mathbf{f}_i} = \delta_s$ for the Gaussian filter and $\delta_{\mathbf{f}_i} = (\delta_s, \delta_r)$ for the bilateral filter. Note that $\mathbf{K}^o = \mathbf{K}^c$ holds true for the Gaussian filter but not true

1. Due to the invariant property of reflectance layer, we have $o_i^r = s_i^r$ and $E^c(\mathbf{o}) = \sum_i (o_i - s_i)^2 = \sum_i (o_i^l - o_i^r + s_i^l - s_i^r)^2 = \sum_i (o_i^l - s_i^l)^2$.



Fig. 3. Visual results of our IIT algorithm with the Gaussian and bilateral filters, respectively. (a) Source, (b) CLAHE exemplar [61], (c) and (d) corresponding results. The noise and distortions are suppressed significantly in comparison to the CLAHE exemplar. TMQI (b)~(d), top: 0.810, 0.903, 0.910, and bottom: 0.845, 0.891, 0.898.

for the bilateral filter, because \mathbf{K}^o is dependent on output image \mathbf{o} and cannot be pre-computed in this case. For simplicity, we set $\mathbf{K} = \mathbf{K}^o = \mathbf{K}^c$ in our experiments.

For the LLE weights, it may be unstable to take a direct solver [47], when the number of neighbors of each point is larger than the space dimension. As described in [49], the matrix \mathbf{W} can be computed by solving the point-wise regularized problem,

$$\min \sum_i (s_i - \sum_{j \in \Omega_i} \omega_{i,j}^s s_j)^2 + \epsilon \|\omega^s\|_2^2, \text{ s.t. } \sum_{j \in \Omega_i} \omega_{i,j}^s = 1. \quad (13)$$

The computational complexity of the LLE algorithm is $O(NDK^3)$ for all the N points with K neighbours in D dimensional space. We refer the reader to some more complex

regularizers such as the modified LLE algorithm [56], in which more robust solutions are given to distribute the contribution of neighbours to each point more uniformly.

After obtaining the \mathbf{K} and \mathbf{W} , Eq.(12) can be solved by setting $dE/do = 0$, giving the following linear system:

$$(\alpha \mathbf{K}^T \mathbf{K} + \beta \mathbf{M}^T \mathbf{M} + \gamma \mathbf{I}) \mathbf{o} = \alpha \mathbf{K}^T \mathbf{K} \mathbf{c} + \gamma \mathbf{s}, \quad (14)$$

where $\mathbf{L} = \alpha \mathbf{K}^T \mathbf{K} + \beta \mathbf{M}^T \mathbf{M} + \gamma \mathbf{I}$ is a large and sparse *Laplacian matrix*. Since \mathbf{L} is symmetric and semi-positive, Eq. (14) can be solved with the solvers such as Gauss-Seidel method and preconditioned conjugate gradients (PCG) method [48]. We use the HSC solver [31] that provides an efficient preconditioning of \mathbf{L} with $O(N)$ time and memory complexity. All steps are summarized in Algorithm 1.

Algorithm 1 Intrinsic image transfer (IIT) algorithm

Input: Images $\{s_i\}_{i=1, \dots, N}$, $\{c_i\}_{i=1, \dots, N}$ and α, β, γ ;

Output: Image $\{o_i\}_{i=1, \dots, N}$;

- 1) **Identifying filters:** \mathbf{K}^o and \mathbf{K}^c
 - a) Set parameters: $\mathcal{N}_i, \delta_s, \delta_r$ or $(\mathcal{N}_i, \delta_s)$;
 - b) Compute $\mathcal{K}_{i,j}$ in Eq. (4) and $\mathbf{K}^o, \mathbf{K}^c$ in Eq. (12);
 - 2) **Computing LLE weights:** \mathbf{W}
 - a) Set parameters: Ω_i, ϵ ;
 - b) Find neighbors Ω_i for each pixel i ;
 - c) Compute $\omega_{i,j}^s$ in Eq. (13);
 - d) Set $\omega_{i,j} = \omega_{i,j}^s$, and $\mathbf{M} = \mathbf{I} - \mathbf{W}$;
 - 3) **Reconstruction**
 - a) Compute the *Laplacian matrix* \mathbf{L} in Eq. (14);
 - b) Solve Eq. (14) with PCG algorithm;
-

4 EXPERIMENTAL RESULTS

In this section, we extensively illustrate the benefits of our IIT algorithm for illumination-related tasks, such as illumination compensation, image enhancement, tone mapping, and HDR image compression. We first interpret how to generate an “exemplar” image and show its robustness to provide global illumination guidance under our IIT framework. Subsequently, the performance of the proposed method is discussed with a series of numerical experiments and quantitative evaluations on different datasets. Our Matlab implementation runs on a desktop PC with an Intel i7 3.40 GHz, 32GB RAM. It takes roughly 3 seconds to process a 600×400 resolution color image. The code is available online: https://github.com/QingXin96/Intrinsic_image_transfer.

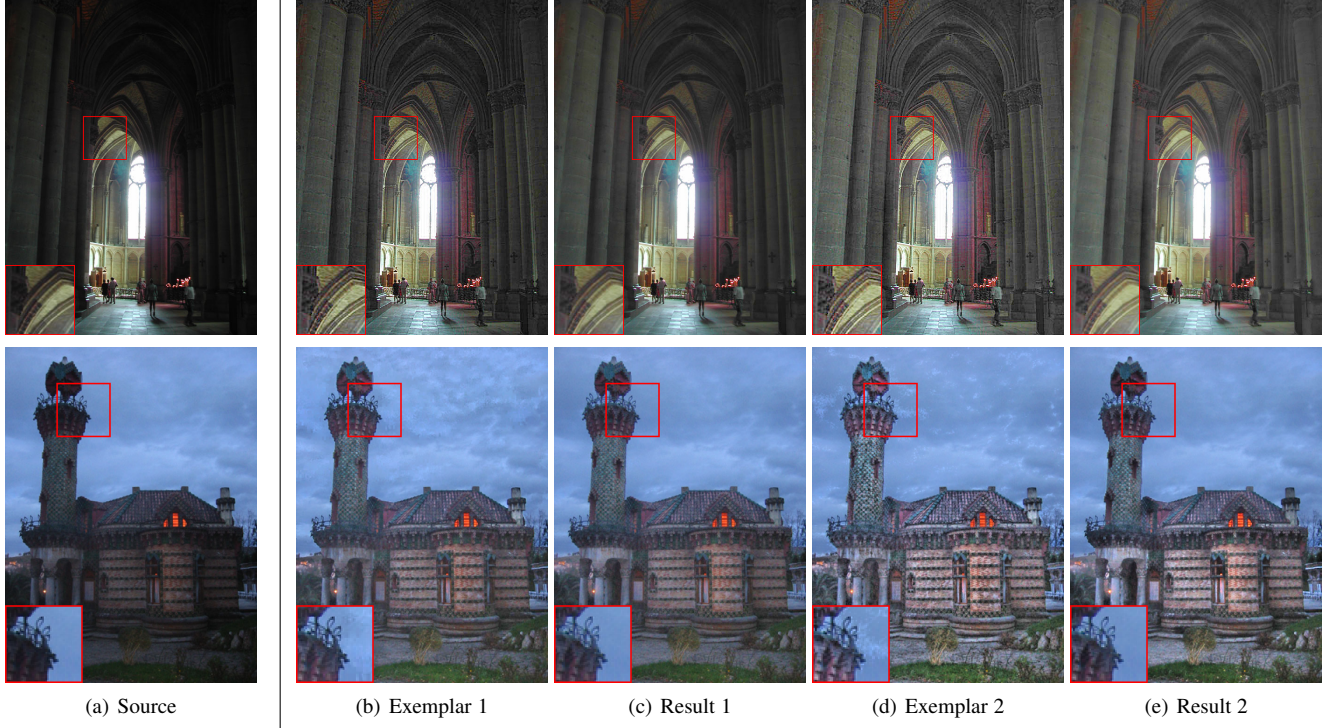


Fig. 4. Visual results of our IIT algorithm by using exemplars with different levels of textural distortions. (a) Source; (b) and (d) exemplars [61] (c) and (e) the corresponding results. TMQI, (b)~(e), top: 0.865, 0.935, 0.832, 0.921; bottom: 0.842, 0.906, 0.827, 0.938.

As explained before, image illumination would deviate from the ideal target in many illumination-related applications. In such cases, an ideal latent target illumination is necessary to our IIT algorithm in theory. However, it is difficult to provide such an illumination layer because it would require a high-quality intrinsic image decomposition. Alternatively, we introduce a pre-computed “exemplar” image to regularize the illumination layer, as explained in Section 3. We claim that such an exemplar is easy-fulfilled under our IIT framework, which helps to simplify the whole scheme significantly, as there is no need to take an ill-posed image decomposition. Notice that local details in the exemplar, no matter in what conditions, would be smoothed by filter kernel \mathcal{K} under the smoothing illumination assumption. This observation implies that one can use an exemplar without caring much about the local details, while an image with fine-balanced global illumination is sufficient to help control the image illumination. As a result, many existing methods can be used to generate such an exemplar for our IIT algorithm. In order to verify the role of exemplar, we here consider two cases: a simple exemplar given by the CLAHE method [61] with fine-balanced global illumination but distorted local details, and a complex one generated by the existing cutting-edge methods, including NASA Retinex [3], Google Nik (GN) [2], Apple Photo Enhancer (APE), Adobe Photoshop CC 2018 [1] and WESPE method [25]. Notice that we only specify the global smoothing illumination property, but our model does not rely on any specified exemplars.

Firstly, we show the results with a CLAHE exemplar. We set $\{\mathcal{N}_i, \delta_s\} = \{5 \times 5, 2.0\}$ and $\{\mathcal{N}_i, \delta_s, \delta_r\} = \{5 \times 5, 2.0, 0.2\}$ for the Gaussian and bilateral filters, respectively. In regard to the LLE weights, we choose $\Omega_i = \{5 \times 5\}$ and $\epsilon = 1e-5$. The global parameters α, β, γ are set to 0.8, 100 and 0.2 respectively. We impose $\alpha + \gamma = 1$ to limit the output results

between the source and exemplar; and a large β is utilized to force the output local textures to be more consistent with the source image. We adopt the default parameter-settings for the CLAHE algorithm [61] as explained therein. As shown in Fig. 3, our IIT algorithm indeed exhibits significant improvements in suppressing the serious noise and distortions, especially in the regions “faces” and “traffic lights” in top row, and around the swan’s “neck” and “wing” of the bottom row. In addition, tiny difference occurs between using the Gaussian filter and bilateral filter.

In addition, we also demonstrate the robustness of our method when using different exemplars. As shown in Fig. 4, two typical exemplars (b) and (d) exhibit different levels of global illumination and textural distortions; and it is notable that our IIT algorithm can produce satisfying results (c) and (e) that has identical global illumination but significantly suppressed local artifacts compared

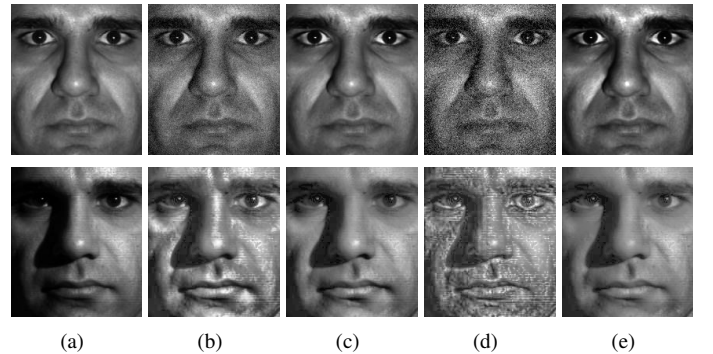


Fig. 5. Illumination compensation on Yale Face dataset [50]. (a) Source, (b) and (d) CLAHE exemplars [61], (c) and (e) results (IIT+ BF). TMQI, top: 0.935, 0.985, 0.833, 0.981; bottom: 0.922, 0.967, 0.897, 0.965.



Fig. 6. Visual comparison on image enhancement. The exemplars in (d) and (h) are produced by the state-of-arts (c) NASA Retinex [3] and (g) GD Compression [15] respectively. TMQI, top (b)~(d): 0.919, 0.943, 0.946; bottom (f)~(h): 0.894, 0.923, 0.934.

with the corresponding exemplars. Moreover, the quality of results drops slightly when increasing the level of local textural distortions in the exemplar. Experimental results indeed illustrate that local artifacts in exemplar are not problematic to our method in general because this textural-inconsistency would receive large penalties and suppressed by the loss functions. For the sake of completeness, we also introduce two strongly degraded exemplars: noise (top) and distortions (bottom²) to show the robustness of our method to the local degraded details in the exemplars. As shown in Fig. 5, our IIT method produce comparable global illumination and also significantly suppress the noise and distortion in the face regions of the exemplars.

Secondly, we validate our algorithm with an exemplar given by the state-of-the-art. In this case, α, β and γ are set to 0.95, $10 \sim 100$ and 0.05. The parameter β may vary according to the level of artifacts in exemplars. This configuration is preferable, as the exemplars reveal better quality with much better balanced global illumination and not so strong local artifacts as produced by CLAHE method. Let $\alpha \gg \gamma$, the output will be much closer to the exemplar. As shown in Fig. 6, we compare the results on NASA Retinex dataset [3]. It is easy to see that our method gives two

results with comparable global illumination but more consistent local textures than NASA Retinex [3] and GD Compression [15]. It is notable that our method attains a similar enhanced result as GD Compression with more visual-friendly color restoration. The NASA Retinex method produces high-quality results with vivid color and contrast but strong noise. In contrast, our IIT method can suppress noise without weakening the color and contrast. This is further verified in Fig. 7, where the local structures of “street lamp” are preserved and the “road” reveals little texture distortions, compared with the impressive WESPE method [25]. Due to the translation-invariant property of the LLE “encoding” model, our IIT algorithm can reconstruct natural-looking results with high-quality consistent local details in these cases.

In order to verify our IIT methods, we further take a quantitative evaluation based on the four datasets: NASA Retinex [3], Kitti [18], Cityscapes [12] and DPED [26]. Notice that the ground truth images are not available in the illumination-related tasks such as image tone mapping, thus it is difficult to take an objective evaluation for our IIT method. We here employ a quantitative evaluation based on the Tone Mapped image Quality Index (TMQI) [54], Integrated Local Natural Image Quality Evaluator (IL-NIQE) [55] and Neural Image Assessment (NIMA) [52]. The TMQI [54] index is a full-reference image assessment between the source and output. In TMQI index, Structural Fidelity (SF) and Statistical

TABLE 1
Quantitative evaluation on NASA Retinex [3], Kitti [18], Cityscapes [12] and DPED [26] datasets.

Method	NASA			Kitti			Cityscapes			DPED		
	(SF / SN) TMQI	IL-NIQE	NIMA	(SF / SN) TMQI	IL-NIQE	NIMA	(SF / SN) TMQI	IL-NIQE	NAMA	(SF / SN) TMQI	IL-NIQE	NIMA
NASA Retinex	(0.916/0.731) 0.937	20.71	4.562	(- / -) -	-	-	(- / -) -	-	-	(- / -) -	-	-
Photoshop CC	(0.948/0.428) 0.892	21.65	4.003	(0.984/0.738) 0.958	23.69	3.818	(0.988/0.323) 0.887	17.37	3.859	(0.982/0.507) 0.916	22.38	4.479
APE	(0.946/0.272) 0.840	24.25	4.002	(0.981/0.618) 0.937	20.91	3.922	(0.980/0.320) 0.884	16.76	4.185	(0.980/0.566) 0.927	21.62	4.613
Google Nik	(0.927/0.527) 0.906	21.32	4.131	(0.968/0.812) 0.965	23.15	3.822	(0.947/0.818) 0.960	18.12	4.092	(0.963/0.567) 0.925	<u>21.53</u>	4.523
WESPE	(- / -) -	-	-	(- / -) -	-	-	(0.915/0.839) 0.956	20.25	4.338	(0.931/0.626) 0.928	22.25	4.534
IIT+GF (Ours)	(0.957/0.650) 0.936	<u>20.62</u>	<u>4.475</u>	(0.981/0.871) 0.976	21.56	<u>3.931</u>	(0.979/0.835) 0.971	4.252	<u>4.313</u>	(0.969/0.587) 0.929	21.95	4.555
IIT+BF (Ours)	(0.960/0.678) 0.942	20.57	4.470	(0.982/0.876) 0.978	21.01	3.935	(0.981/0.826) 0.970	16.48	4.293	(0.973/0.589) 0.931	21.31	4.540

2. We set the parameters: “ClipLimit = 0.01” and “NumTiles = 16×16 ” to get the better global illumination as interpreted in CLAHE [61].

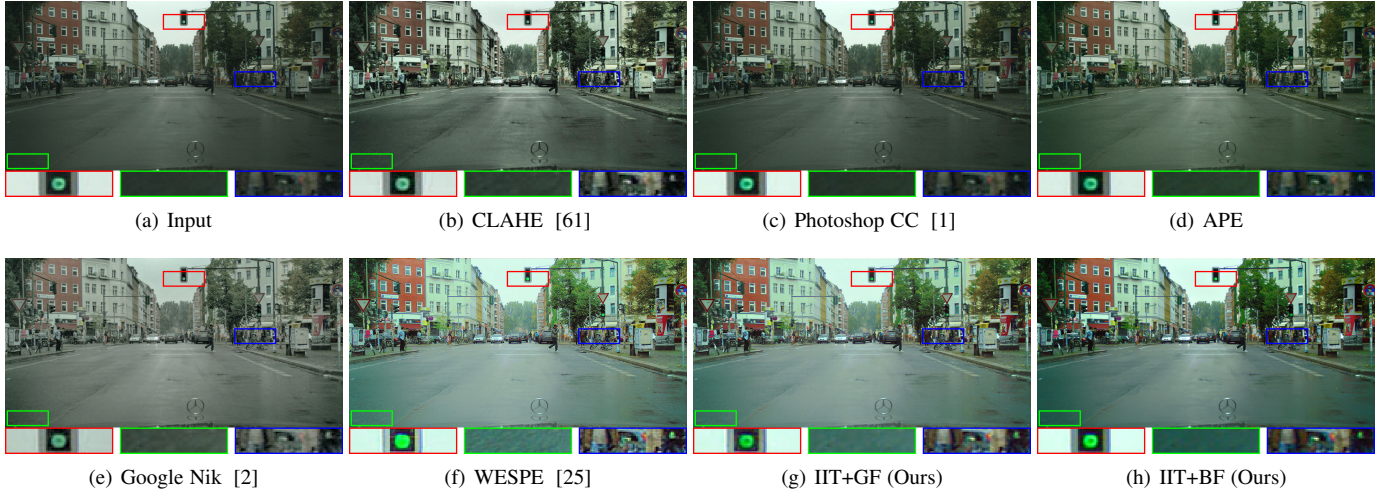


Fig. 7. Visual comparison on Cityscapes dataset [12]. The exemplars used in (g) and (h) are given by the state-of-art (f) WESPE [25]. TMQI, (b)~(h): 0.891, 0.913, 0.973, 0.893, 0.801, 0.921, 0.942.

Naturalness (SN) are considered to provide an objective quality assessment. The SF index is to extract structural information from the visual scene and provides a perceptual predictor of structural fidelity. The SN index is a statistic metric on output image, and it takes more image attributes such as brightness, contrast, visibility and details into account. IL-NIQE [55] and NIMA [52] are two no-reference image assessments. The IL-NIQE index is a learning-based method integrating natural image statistics features derived from image color, luminance, gradient and structure information. While the NIMA index attempts to predict consistent aesthetic scores with human opinions using convolutional neural networks. The statistical results are shown in Table 1. Top two results are highlighted with **bold** and underline, respectively. The benefits are noticeable with total 15 top-two places in 24 indices comparing with the state-of-art in real-world datasets.

Our algorithm can be extended to high dynamic range (HDR) image compression to improve the visibility of dark regions. In particular, it can help to suppress the distorted details or artifacts generated by these prevailing methods such as gradient-domain (GD) compression [15] and weighted least square (WLS) filter [14]. We deal with the image luminance based on the same aforementioned configurations. The saturation is restored with a heuristic de-saturation setup as described in [15].

$$C_{out} = \left(\frac{C_{in}}{L_{in}} \right)^s L_{out}, \quad (15)$$

where $C = \{R, G, B\}$ are red, green and blue channels of color images, L_{in} and L_{out} denote the source and mapped luminance, and s controls the saturation with an empirical value between 0.4 and 0.6 to produce satisfying results.

5 CONCLUSION

This paper has described a new intrinsic image transfer algorithm, which is rather different from the recent trends towards making an intrinsic image decomposition. This model creates a local image translation between two image surfaces and produces high-quality results in a wide range of illumination manipulation tasks. One drawback is that the algorithm is time-consuming for the need of computing the large-scale LLE weights and PCG solver. We will address them with a sub-sampling strategy for efficiency.

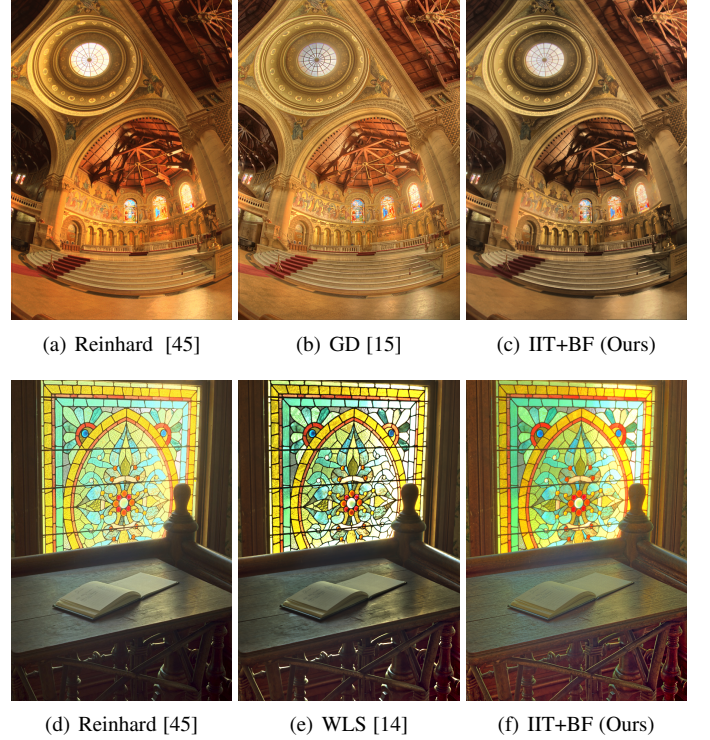


Fig. 8. Visual comparison of the HDR image compression with the CLAHE exemplars [61]. TMQI, top (a)~(c): 0.943, 0.948, 0.928; bottom (d)~(f): 0.902, 0.940, 0.953.

ACKNOWLEDGMENTS

The authors would like to thank to the online resources, including images, code and so on. This work was supported in part by the National Science and Technology Major Project (J2019-V-0010-0104) and Shandong MSTI Project (2019JZZY010122), China and also partially supported by the FWO Odysseus Project, Leverhulme Grant RPG-2017-151 and EPSRC grant EP/R003025/1. The authors are grateful to Prof. Michael Ruzhansky for his salient comments and suggestions.

REFERENCES

- [1] Adobe photoshop cc. <https://www.adobe.com/cn/products/photoshop.html/>.
- [2] Google nikcollection. <https://www.google.com/nikcollection/>.
- [3] Nasa retinex. <https://dragon.larc.nasa.gov/retinex/>.
- [4] Jonathan T Barron and Jitendra Malik. Shape, illumination, and reflectance from shading. *IEEE transactions on pattern analysis and machine intelligence*, 37(8):1670–1687, 2015.
- [5] Harry Barrow and J Tenenbaum. Recovering intrinsic scene characteristics. *Comput. Vis. Syst.*, 2, 1978.
- [6] Sean Bell, Kavita Bala, and Noah Snavely. Intrinsic images in the wild. *ACM Transactions on Graphics (TOG)*, 33(4):159, 2014.
- [7] Sai Bi, Xiaoguang Han, and Yizhou Yu. An l1 image transform for edge-preserving smoothing and scene-level intrinsic decomposition. *ACM Transactions on Graphics (TOG)*, 34(4):78, 2015.
- [8] Daniel J Butler, Jonas Wulff, Garrett B Stanley, and Michael J Black. A naturalistic open source movie for optical flow evaluation. In *European conference on computer vision*, pages 611–625. Springer, 2012.
- [9] Chen Chen, Qifeng Chen, Jia Xu, and Vladlen Koltun. Learning to see in the dark. *arXiv preprint arXiv:1805.01934*, 2018.
- [10] Yu-Sheng Chen, Yu-Ching Wang, Man-Hsin Kao, and Yung-Yu Chuang. Deep photo enhancer: Unpaired learning for image enhancement from photographs with gans. In *Proceedings of the IEEE Conference on Computer Vision and Pattern Recognition*, pages 6306–6314, 2018.
- [11] Lechao Cheng, Chengyi Zhang, and Zicheng Liao. Intrinsic image transformation via scale space decomposition. In *Proceedings of the IEEE Conference on Computer Vision and Pattern Recognition (CVPR)*, pages 656–665, 2018.
- [12] Marius Cordts, Mohamed Omran, Sebastian Ramos, Timo Rehfeld, Markus Enzweiler, Rodrigo Benenson, Uwe Franke, Stefan Roth, and Bernt Schiele. The cityscapes dataset for semantic urban scene understanding. In *Proceedings of the IEEE Conference on Computer Vision and Pattern Recognition (CVPR)*, 2016.
- [13] Michael Elad. Retinex by two bilateral filters. In *International Conference on Scale-Space Theories in Computer Vision*, pages 217–229. Springer, 2005.
- [14] Zeev Farbman, Raanan Fattal, Dani Lischinski, and Richard Szeliski. Edge-preserving decompositions for multi-scale tone and detail manipulation. In *ACM Transactions on Graphics (TOG)*, volume 27, page 67. ACM, 2008.
- [15] Raanan Fattal, Dani Lischinski, and Michael Werman. Gradient domain high dynamic range compression. In *ACM transactions on graphics (TOG)*, volume 21, pages 249–256. ACM, 2002.
- [16] Xueyang Fu, Delu Zeng, Yue Huang, Xiao-Ping Zhang, and Xinghao Ding. A weighted variational model for simultaneous reflectance and illumination estimation. In *Proceedings of the IEEE Conference on Computer Vision and Pattern Recognition (CVPR)*, pages 2782–2790, 2016.
- [17] Marc-André Gardner, Kalyan Sunkavalli, Ersin Yumer, Xiaohui Shen, Emiliano Gambaretto, Christian Gagné, and Jean-François Lalonde. Learning to predict indoor illumination from a single image. *ACM Transactions on Graphics (TOG)*, 36(6):176, 2017.
- [18] Andreas Geiger, Philip Lenz, Christoph Stiller, and Raquel Urtasun. Vision meets robotics: The kitti dataset. *The International Journal of Robotics Research*, 32(11):1231–1237, 2013.
- [19] Alan Gilchrist. *Seeing black and white*. OUP USA, 2006.
- [20] Ian Goodfellow, Jean Pouget-Abadie, Mehdi Mirza, Bing Xu, David Warde-Farley, Sherjil Ozair, Aaron Courville, and Yoshua Bengio. Generative adversarial nets. In *Proceedings of Advances in neural information processing systems (NIPS)*, pages 2672–2680, 2014.
- [21] Xiaojie Guo, Yu Li, and Haibin Ling. Lime: Low-light image enhancement via illumination map estimation. *IEEE transactions on image processing*, 26(2):982–993, 2017.
- [22] Yannick Hold-Geoffroy, Kalyan Sunkavalli, Sunil Hadap, Emiliano Gambaretto, and Jean-François Lalonde. Deep outdoor illumination estimation. In *Proceedings of the IEEE Conference on Computer Vision and Pattern Recognition (CVPR)*, volume 2, 2017.
- [23] Berthold KP Horn. Determining lightness from an image. *Computer graphics and image processing*, 3(4):277–299, 1974.
- [24] Qian Huang, Weixin Zhu, Yang Zhao, Linsen Chen, Yao Wang, Tao Yue, and Xun Cao. Multispectral image intrinsic decomposition via low rank constraint. *arXiv preprint arXiv:1802.08793*, 2018.
- [25] Andrey Ignatov, Nikolay Kobyshev, Radu Timofte, Kenneth Vanhoey, and Luc Van Gool. Wespe: weakly supervised photo enhancer for digital cameras. In *Proceedings of the IEEE Conference on Computer Vision and Pattern Recognition Workshops*, pages 691–700, 2018.
- [26] Andrey Ignatov, Nikolay Kobyshev, Kenneth Vanhoey, Radu Timofte, and Luc Van Gool. Dslr-quality photos on mobile devices with deep convolutional networks. In *Proceedings of the International Conference on Computer Vision (ICCV)*, 2017.
- [27] Junho Jeon, Sunghyun Cho, Xin Tong, and Seungyong Lee. Intrinsic image decomposition using structure-texture separation and surface normals. In *In Proceedings of the European Conference on Computer Vision (ECCV)*, pages 218–233. Springer, 2014.
- [28] Yifan Jiang, Xinyu Gong, Ding Liu, Yu Cheng, Chen Fang, Xiaohui Shen, Jianchao Yang, Pan Zhou, and Zhangyang Wang. Enlighten: Deep light enhancement without paired supervision. *arXiv preprint arXiv:1906.06972*, 2019.
- [29] Daniel J Jobson, Zia-ur Rahman, and Glenn A Woodell. A multiscale retinex for bridging the gap between color images and the human observation of scenes. *IEEE Transactions on Image processing*, 6(7):965–976, 1997.
- [30] Ron Kimmel, Michael Elad, Doron Shaked, Renato Keshet, and Irwin Sobel. A variational framework for retinex. *International Journal of computer vision(IJCV)*, 52(1):7–23, 2003.
- [31] Dilip Krishnan, Raanan Fattal, and Richard Szeliski. Efficient preconditioning of laplacian matrices for computer graphics. *ACM Transactions on Graphics (TOG)*, 32(4):142, 2013.
- [32] Alex Krizhevsky, Ilya Sutskever, and Geoffrey E Hinton. Imagenet classification with deep convolutional neural networks. In *Proceedings of Advances in neural information processing systems (NIPS)*, pages 1097–1105, 2012.
- [33] Edwin H Land. The retinex theory of color vision. *Scientific American*, 237(6):108–129, 1977.
- [34] Edwin H Land. Recent advances in retinex theory and some implications for cortical computations: color vision and the natural image. *Proceedings of the national academy of sciences of the United States of America*, 80(16):5163, 1983.
- [35] Edwin H Land and John J McCann. Lightness and retinex theory. *Josa*, 61(1):1–11, 1971.
- [36] Zhengqi Li and Noah Snavely. Learning intrinsic image decomposition from watching the world. In *Proceedings of the IEEE Conference on Computer Vision and Pattern Recognition (CVPR)*, pages 9039–9048, 2018.
- [37] Jiaying Liu, Dejia Xu, Wenhan Yang, Minhao Fan, and Haofeng Huang. Benchmarking low-light image enhancement and beyond. *International Journal of Computer Vision*, 129(4):1153–1184, 2021.
- [38] Stephen Lombardi and Ko Nishino. Radiometric scene decomposition: Scene reflectance, illumination, and geometry from rgb-d images. In *3D Vision (3DV), 2016 Fourth International Conference on*, pages 305–313. IEEE, 2016.
- [39] Wenye Ma, Jean-Michel Morel, Stanley Osher, and Aichi Chien. An l1-based variational model for retinex theory and its application to medical images. In *Proceedings of the IEEE Conference on Computer Vision and Pattern Recognition (CVPR)*, pages 153–160, 2011.
- [40] Rafał K Mantiuk, Karol Myszkowski, and Hans-Peter Seidel. *High dynamic range imaging*. Wiley Online Library, 2015.
- [41] Abhimitra Meka, Maxim Maximov, Michael Zollhöfer, Avishek Chatterjee, Hans-Peter Seidel, Christian Richardt, and Christian Theobalt. Lime: Live intrinsic material estimation. In *Proceedings of the IEEE Conference on Computer Vision and Pattern Recognition (CVPR)*, pages 6315–6324, 2018.
- [42] Ján Morovic and M Ronnier Luo. The fundamentals of gamut mapping: A survey. *Journal of Imaging Science and Technology*, 45(3):283–290, 2001.
- [43] Takuya Narihira, Michael Maire, and Stella X Yu. Direct intrinsics: Learning albedo-shading decomposition by convolutional regression. In *Proceedings of the International Conference on Computer Vision (ICCV)*, pages 2992–2992, 2015.
- [44] Michael K Ng and Wei Wang. A total variation model for retinex. *SIAM Journal on Imaging Sciences*, 4(1):345–365, 2011.
- [45] Erik Reinhard, Michael Stark, Peter Shirley, and James Ferwerda. Photographic tone reproduction for digital images. *ACM transactions on graphics (TOG)*, 21(3):267–276, 2002.
- [46] Carsten Rother, Martin Kiefel, Lumin Zhang, Bernhard Schölkopf, and Peter V Gehler. Recovering intrinsic images with a global sparsity prior on reflectance. In *Proceedings of Advances in neural information processing systems (NIPS)*, pages 765–773, 2011.
- [47] Sam T Roweis and Lawrence K Saul. Nonlinear dimensionality reduction by locally linear embedding. *Science*, 290(5500):2323–2326, 2000.
- [48] Yousef Saad. *Iterative methods for sparse linear systems*, volume 82. SIAM, 2003.

- [49] Lawrence K Saul and Sam T Roweis. Think globally, fit locally: unsupervised learning of low dimensional manifolds. *Journal of machine learning research*, 4(Jun):119–155, 2003.
- [50] Florian Schroff, Tali Treibitz, David Kriegman, and Serge Belongie. Pose, illumination and expression invariant pairwise face-similarity measure via doppelgänger list comparison. In *Proceedings of the International Conference on Computer Vision (ICCV)*, pages 2494–2501. IEEE, 2011.
- [51] Li Shen and Chuohao Yeo. Intrinsic images decomposition using a local and global sparse representation of reflectance. 2011.
- [52] Hossein Talebi and Peyman Milanfar. Nima: Neural image assessment. *IEEE Transactions on Image Processing*, 27(8):3998–4011, 2018.
- [53] Carlo Tomasi and Roberto Manduchi. Bilateral filtering for gray and color images. In *Computer Vision, 1998. Sixth International Conference on*, pages 839–846. IEEE, 1998.
- [54] Hojatollah Yeganeh and Zhou Wang. Objective quality assessment of tone-mapped images. *IEEE transactions on image processing*, 22(2):657–667, 2013.
- [55] Lin Zhang, Lei Zhang, and Alan C Bovik. A feature-enriched completely blind image quality evaluator. *IEEE transactions on image processing*, 24(8):2579–2591, 2015.
- [56] Zhenyue Zhang and Jing Wang. Mlle: Modified locally linear embedding using multiple weights. In *Proceedings of Advances in neural information processing systems (NIPS)*, pages 1593–1600, 2007.
- [57] Qi Zhao, Ping Tan, Qiang Dai, Li Shen, Enhua Wu, and Stephen Lin. A closed-form solution to retinex with nonlocal texture constraints. *IEEE transactions on pattern analysis and machine intelligence*, 34(7):1437–1444, 2012.
- [58] Yinqiang Zheng, Imari Sato, and Yoichi Sato. Illumination and reflectance spectra separation of a hyperspectral image meets low-rank matrix factorization. In *Proceedings of the IEEE Conference on Computer Vision and Pattern Recognition (CVPR)*, pages 1779–1787, 2015.
- [59] Jun-Yan Zhu, Taesung Park, Phillip Isola, and Alexei A Efros. Unpaired image-to-image translation using cycle-consistent adversarial networks. In *Proceedings of the IEEE international conference on computer vision*, pages 2223–2232, 2017.
- [60] Dominique Zosso, Giang Tran, and Stanley J Osher. Non-local retinex—a unifying framework and beyond. *SIAM Journal on Imaging Sciences*, 8(2):787–826, 2015.
- [61] Karel Zuiderveld. Contrast limited adaptive histogram equalization. *Graphics gems*, pages 474–485, 1994.



Qianying Zhang received the BS degree in Mathematics from Zhengzhou University, Zhengzhou, China, in 2011, and the PhD degree in Mathematics from Beihang University (BUAA), Beijing, China, in 2015. She is in Shenzhen Institute of Information Technology. Her research interests include signal and image processing, compressed sensing, sparse representation and artificial intelligence.



Haihui Wang received the PhD degree in Mathematics from Beijing University, Beijing, China, in 2003. She is currently an Associate Professor in the School of Mathematical Sciences, Beihang University (BUAA), Beijing, China, and an Associate Professor in the Health Science Center, Beijing University, Beijing, China. Her research interests include artificial intelligence, machine learning, signal and image processing, wavelet analysis and application, and so on.



Junqing Huang received the BS degree in Automation from the School of Electrical Engineering, Zhengzhou University, Zhengzhou, China, in 2011, and the MS degree in Mathematics from the School of Mathematical Sciences, Beihang University (BUAA), Beijing, China, in 2015. He is currently a Ph.D. candidate of Department of Mathematics: Analysis, Logic and Discrete Mathematics, Ghent University, Belgium. His research interests include deep learning, image processing, optimal transport and optimization.



Michael Ruzhansky is currently a senior full Professor in Department of Mathematics and a Professorship in Special Research Fund (BOF) at Ghent University, Belgium, a Professorship in School of Mathematical Sciences at Queen Mary University of London, UK, and Honorary Professorship in Department of Mathematics at Imperial College London, UK. He was awarded by FWO (Belgium) the prestigious Odysseus 1 Project in 2018, he was recipient of several Prizes and Awards: ISAAC Award in 2007, Daiwa Adrian Prize in 2010 and Ferran Sunyer I Balaguer Prizes in 2014 and 2018. His research interests include different areas of analysis, in particular, theory of PDEs, microlocal analysis, and harmonic analysis.